Optimal Power Flow with Large-Scale Storage Integration

Dennice Gayme, *Member, IEEE* and Ufuk Topcu, *Member, IEEE*

***Abstract*—Restructuring of the electric power industry along with mandates to integrate renewable energy sources is introducing new challenges for the electric power system. Intermittent power sources in particular, require mitigation strategies in order to maintain consistent power on the electric grid. We investigate distributed energy storage as one such strategy. Our model for optimal power flow with storage augments the usual formulation by adding simple charge/discharge dynamics for energy storage collocated with load and/or generation buses cast as a finite-time optimal control problem. We first propose a solution strategy that uses a convex optimization based relaxation to solve the optimal control problem. We then use this framework to illustrate the effects of various levels of energy storage using the topology of the IEEE 14 bus benchmark system along with both time-invariant and demand-based cost functions. The addition of energy storage and demand-based cost functions significantly reduces the generation costs and flattens the generation profiles.**

***Index Terms*—Distributed power generation; electric power dispatch; energy storage; optimization methods; power system analysis; power system control.**

I. Introduction

Electric power systems and the power grid are currently undergoing a restructuring due to a number of factors such as increasing demand, additional uncertainty caused by the integration of intermittent renewable energy sources and further deregulation of the industry [2], [9], [11]. The integration of renewables in particular is being accelerated by government mandates, e.g., see [35] which details these directives for 30 US states. The operational challenges associated with these trends can be alleviated by effectively utilizing grid-integrated distributed energy storage [6]. The potential benefits of grid-integrated storage technologies include decreasing the need for new transmission or generation capacity, improving load following, providing spinning reserve, correcting frequency, voltage, and power factors, as well as the indirect environmental advantages gained through facilitating an increased penetration of renewable energy sources [30].

The promise of effective grid-integrated energy storage schemes is widely accepted and this has led to a great deal of research activity [16]. We give a brief overview of some of the past work as it ties to the problem studied here (a thorough survey is beyond the scope of this paper). The role of storage in power regulation and peak-shaving was studied through simulation as early as 1981 [38]. More recently, the utility of energy storage in mitigating the effects of integration of renewable resources has been investigated in both traditional [3], [15], [17] and micro-grid [32] settings. Reference [6] used a probabilistic model to predict the feasibility of increased renewable penetration given different types, sizes, and time scales of storage technologies. The effect of energy storage on various performance metrics, such as, the probability of load-shedding, has also been investigated through the use of different combinations of hybrid generation (i.e., a combination of wind, solar and fossil fuel based generation systems) versus storage capacities. See [37] and the references therein for the special case of an isolated system, e.g., a power system for an island with no mainland connection. Economic questions, such as, how to increase the value of storage device ownership [36] and how to efficiently allocate energy storage to minimize curtailed wind energy (in a system with a high penetration of wind generation) [4], have also been studied. However, there are still many questions that need to be addressed to understand the full potential and limitations of large-scale energy storage. In particular, the appropriate storage technology along with the required capacity and rates of charge/discharge are the subject of continuing research [29]. The present work uses an optimal power flow formulation that includes storage charge/discharge dynamics to investigate how different storage capacities affect peak-shaving and other performance metrics using a case study based on the IEEE 14 benchmark system [34].

The optimal power flow (OPF) problem [13], [14], [18], [26] optimizes a cost function, e.g., generation cost and/or user utilities, over variables such as real and reactive power outputs, voltages, and phase angles at a number of buses subject to capacity and network constraints. It has been extensively studied since the pioneering work of Carpentier [10]. The surveys in [19], [27], [28] provide a historical overview of special instances of the problem and various solution strategies. More recent work has focused on potentially restrictive yet computationally more tractable instances and reformulations of the problem. For example, references [20], [21] considered radial distribution systems as conic programming problems. The problem was first formulated as a semi-definite program (SDP) in [5]. This idea was further refined and extensively analyzed in [22]–[24], where a sufficient condition under which there is an equivalent convex relaxation that provides an exact solution to the OPF problem was provided and proved.

The formulation in this paper extends the OPF problem formulation in [23], [24] to integrate simple charge/discharge dynamics for energy storage distributed over the network. The inclusion of these storage dynamics leads to a finite-horizon optimal control problem that enables optimization of power allocation over time in addition to static allocation over the network. The current formulation augments the ideas presented in [12] through elimination of the small-angle assumption and the addition of power rate limits on the energy storage. The

This work was partially supported by the Boeing Corporation and AFOSR (FA9550-08-1-0043).

D. Gayme is with the Department of Mechanical Engineering at the Johns Hopkins University, Baltimore, MD, USA, 21218 and U. Topcu is with the Department of Computing and Mathematical Sciences, California Institute of Technology, Pasadena, CA, USA, 91125. dennice@jhu.edu, utopcu@cds.caltech.edu

expanded problem setting allows us to evaluate how changes in storage capacity, power rating, and distribution over the network affect performance metrics such as cost and peak generation.

The contributions of this paper are twofold. First, it proposes a formulation for OPF with storage dynamics along with a strategy to relatively efficiently (i.e., with provably polynomial complexity) compute its optimal solution. The procedure and solution method, both described in Section III, extend the SDP relaxations described in [5], [23], [24] to allow the inclusion of simple storage dynamics. Second, this computational procedure is used to investigate the effects of different energy storage capacities on generation costs and peak-shaving using an IEEE benchmark network [34] as an example. As an initial step, we neglect uncertainties due to fluctuations in demand and/or intermittency in generation.

II. Problem setup

Consider a power network with n buses and $m \leq n$ generators. Define $\mathcal{N} := \{1, \ldots, n\}$ and $\mathcal{G} := \{1, \ldots, m\}$ as the set of indices of all buses and the generator buses, respectively. Let $Y \in \mathbb{C}^{n \times n}$ be the admittance matrix defining the underlying network topology as described in [26], [39]. In the following, we extend an OPF problem formulation from [26] to include simple dynamics for storage units located at each of the buses. See Figure 1 for a sample network structure augmented with storage units, which is also used in Section IV. Note that the terms bus and node are used interchangeably throughout the remainder of this paper.

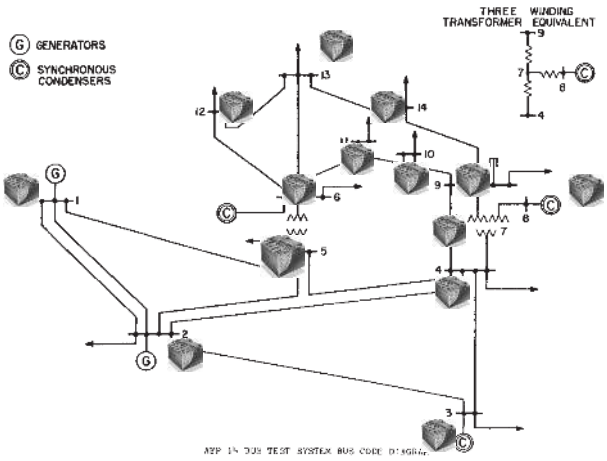

Fig. 1. Topology of the IEEE 14 bus test case with energy storage units (depicted as batteries in the figure) at each node. This figure is a modified version of the figure provided in [34].

The active and reactive power generation $P_l^g(t)$ and $Q_l^g(t)$ at generation buses $l \in \mathcal{G}$ for times $t \in \mathcal{T} := \{1, \ldots, T\}$ are respectively bounded as

$$P_l^{min} \leq P_l^g(t) \leq P_l^{max}, \tag{1a}$$
$$Q_l^{min} \leq Q_l^g(t) \leq Q_l^{max}. \tag{1b}$$

The voltage magnitude $V_k(t)$ at bus $k \in \mathcal{N}$ and time $t \in \mathcal{T}$ is bounded as

$$V_k^{min} \leq |V_k(t)| \leq V_k^{max}. \tag{2}$$

At bus $k \in \mathcal{N}$, let $b_k(t)$ denote the amount of energy storage at time $t \in \mathcal{T}$ and $r_k(t)$ denote the rate of charge/discharge of energy at time $t = 1, \ldots, T-1$. The amount of storage at bus $k \in \mathcal{N}$ is modeled to follow the first-order difference equation

$$b_k(t+1) = b_k(t) + r_k(t)\Delta t, \quad \text{for } t = 1, \ldots, T-1, \tag{3}$$

where Δt denotes the time interval $[t, t+1]$ and the initial condition is given by

$$b_k(1) = \mathfrak{g}_k. \tag{4}$$

The amount of storage $b_k(t)$ and its rate $r_k(t)$ of charge/discharge, at each bus $k \in \mathcal{N}$, are bounded as

$$0 \leq b_k(t) \leq B_k^{max}, \quad \text{for } t \in \mathcal{T} \tag{5a}$$
$$R_k^{min} \leq r_k(t) \leq R_k^{max}, \quad \text{for } t = 1, \ldots, T-1. \tag{5b}$$

The network constraints at each $k \in \mathcal{N}$ and time $t \in \mathcal{T}$, are

$$\begin{aligned} V_k(t) I_k^*(t) = {} & P_k^g(t) - P_k^d(t) - r_k(t) \\ & + \left[Q_k^g(t) - Q_k^d(t) - s_k(t) \right] \mathbf{i}, \end{aligned} \tag{6}$$

where $s_k(t)$ is the reactive storage power inflow/outflow at bus $k \in \mathcal{N}$ and time $t \in \mathcal{T}$, which is bounded as

$$S_k^{min} \leq s_k(t) \leq S_k^{max}. \tag{7}$$

We use the convention that $P_k^g(t) = Q_k^g(t) = 0$ for $k \in \mathcal{N} \backslash \mathcal{G}$ and $t \in \mathcal{T}$ and $r_k(T) = 0$ and $s_k(T) = 0$ for $k \in \mathcal{N}$. Combining the above expressions results in the following OPF problem with storage dynamics.

$$\begin{aligned} \varphi^* := \min \quad & \sum_{t=1}^{T} \sum_{l \in \mathcal{G}} c_{l2}(t) \left(P_l^g(t) \right)^2 + c_{l1}(t) P_l^g(t) \\ \text{subject to} \quad & \\ & (1),\ (2),\ (3),\ (4),\ (5),\ (6),\ \text{and } (7) \end{aligned} \tag{8}$$

over the decision variables $V_k(t)$, $P_k^g(t)$, $Q_k^g(t)$, $b_k(t)$, $r_k(t)$, and $s_k(t)$ (with the respective bus and time indices k and t running over the sets specified above).

The conventional OPF problem has no correlation across time; therefore, the corresponding optimization is static and can be solved independently at each time. The addition of storage charge/discharge dynamics allows optimization across time, i.e., the ability to charge when the cost of generation is low and discharge when it is high. The admittance matrix induces optimization across the network in both formulations.

III. Solution strategy

The nonconvexity of the constraint (2) and the bilinearity in the equality constraint in (6) make the general problem in (8) nonconvex. In this section we propose a convex relaxation of (8) following a procedure similar to that discussed in [23], [24] and show that the addition of storage dynamics does not change the overall structure of the dual problem. Therefore, the same assumptions that are presented in those works allow a solution for (8) to be constructed from the Lagrangian dual of the relaxation. Section III-B provides a procedure for constructing a solution for the OPF problem with storage dynamics from that of the dual problem.

A. Lagrangian relaxation for the OPF problem with storage

In order to define the Lagrangian relaxation of the optimization of the OPF with storage we first reformulate the problem following the procedure described in [23], [24] and partially adopt their notation. Let $U(t) := [\text{Re}(V(t)), \text{Im}(V(t))]^T$, $W(t) := U(t)U(t)^T$ and $Y_k := e_k e_k^* Y$, where $e_k \in \mathbb{R}^n$, $k = 1, \ldots, n$, is the standard basis vectors for $\mathbb{R}^n$ and $\text{Re}(\cdot)$ and $\text{Im}(\cdot)$ denote the real and imaginary parts of their arguments, respectively. Define

$$M_k := \begin{bmatrix} e_k e_k^* & 0 \\ 0 & e_k e_k^* \end{bmatrix},$$

$$\mathbf{Y}_k := \frac{1}{2} \begin{bmatrix} \text{Re}\{Y_k + Y_k^T\} & \text{Im}\{Y_k^T - Y_k\} \\ \text{Im}\{Y_k - Y_k^T\} & \text{Re}\{Y_k + Y_k^T\} \end{bmatrix}, \text{ and}$$

$$\overline{\mathbf{Y}}_k := -\frac{1}{2} \begin{bmatrix} \text{Im}\{Y_k + Y_k^T\} & \text{Re}\{Y_k - Y_k^T\} \\ \text{Re}\{Y_k^T - Y_k\} & \text{Im}\{Y_k + Y_k^T\} \end{bmatrix}.$$

Then the optimization in (8) can be shown to be equivalent to

$$\varphi^* := \min_{W(t),\alpha(t),b(t),r(t),s(t)} \sum_{t=1}^{T} \sum_{l \in \mathcal{G}} \alpha_l(t) \tag{9}$$

subject to

$$P_k^{min} - P_k^d(t) \leq \text{tr}\{\mathbf{Y}_k W(t)\} + r_k(t) \leq P_k^{max} - P_k^d(t), \tag{10a}$$

$$Q_k^{min} - Q_k^d(t) \leq \text{tr}\{\overline{\mathbf{Y}}_k W(t)\} + s_k(t) \leq Q_k^{max} - Q_k^d(t), \tag{10b}$$

$$\left(V_k^{min}\right)^2 \leq \text{tr}\{M_k W(t)\} \leq (V_k^{max})^2, \tag{10c}$$

$$0 \leq b_k(t) \leq B_k^{max}, \tag{10d}$$

$$R_k^{min} \leq r_k(t) \leq R_k^{max}, \tag{10e}$$

$$S_k^{min} \leq s_k(t) \leq S_k^{max}, \tag{10f}$$

$$b_k(t+1) = r_k(t) + b_k(t), \tag{10g}$$

$$b_k(1) = \mathfrak{g}_k, \tag{10h}$$

$$\begin{bmatrix} a_{l0}(t) & a_{l1}(t) \\ a_{l1}(t) & -1 \end{bmatrix} \preceq 0, \tag{10i}$$

$$W(t) \succeq 0, \tag{10j}$$

$$\text{rank}(W(t)) = 1, \tag{10k}$$

where

$$a_{l0}(t) := c_{l1}(t) \left[\text{tr}\{\mathbf{Y}_l W(t)\} + r_l(t) + P_l^d(t)\right] - \alpha_l(t),$$

$$a_{l1}(t) := \sqrt{c_{l2}(t)} \left[\text{tr}\{\mathbf{Y}_l W(t)\} + r_l(t) + P_l^d(t)\right],$$

$l \in \mathcal{G}$, $k \in \mathcal{N}$ and $t \in \mathcal{T}$ for all equations except (10g) where t runs over $\{1, \ldots, T-1\}$. Also, $P_k^g(t) = 0$ and $Q_k^g(t) = 0$ for $k \in \mathcal{N} \backslash \mathcal{G}$ and $t \in \mathcal{T}$ with $r_k(T) = 0$ and $s_k(T) = 0$ for $k \in \mathcal{N}$. For a symmetric matrix X, $X \succeq 0$ ($X \preceq 0$) means that X is positive (negative) semi-definite. The equivalence of (10i) and $c_{l2}(t) \left(P_l^g(t)\right)^2 + c_{l1}(t) P_l^g(t) \leq \alpha_l(t)$ can be shown using the Schur complement formula [8]. The change of variables that transforms (8) into (9)-(10) follows from the fact that a symmetric matrix $X \in \mathbb{R}^{n \times n}$ is positive semi-definite and of rank 1 if and only if there exists $x \in \mathbb{R}^n$ such that $X = xx^T$. Finally, note that (9)-(10) has a linear cost function and convex constraints (linear equality and inequality constraints in (10a)-(10h) and linear matrix inequalities in (10i)-(10j)), except for the nonconvex constraint (10k).

Remark 1: Constraints such as power flow and thermal line limits can easily be added to this formulation using a procedure similar to that in [24]. This will not change the essence of the modeling framework or problem solving techniques but does require a great deal of additional notation, hence it is omitted here for clarity of exposition.

The Lagrangian dual for optimization (9)-(10) excluding the nonconvex rank constraint (10k) can now be stated as

$$\psi^* := \max_{x \succeq 0, z, \sigma, \beta} h(x, z, \sigma, \beta) \tag{11}$$

subject to

$$\sum_{k \in \mathcal{N}} \left[\Lambda_k(t) \mathbf{Y}_k + H_k(t) \overline{\mathbf{Y}}_k + \Upsilon_k(t) M_k\right] \succeq 0, \tag{12a}$$

$$H_k(t) + \xi_k^{max}(t) - \xi_k^{min}(t) = 0, \tag{12b}$$

$$\Lambda_k(t) + \rho_k^{max}(t) - \rho_k^{min}(t) + \sigma_k(t+1) = 0, \tag{12c}$$

$$\sigma_k(t+1) - \sigma_k(t) + \gamma_k^{max}(t) - \gamma_k^{min}(t) = 0, \tag{12d}$$

$$\sigma_k(2) + \gamma_k^{max}(1) - \gamma_k^{min}(1) + \beta_k = 0, \tag{12e}$$

$$-\sigma_k(T) + \gamma_k^{max}(T) - \gamma_k^{min}(T) = 0, \tag{12f}$$

$$\begin{bmatrix} 1 & z_{l1}(t) \\ z_{l1}(t) & z_{l2}(t) \end{bmatrix} \succeq 0, \tag{12g}$$

with $k \in \mathcal{N}$ and $l \in \mathcal{G}$. For (12a), (12b) and (12g) $t \in \mathcal{T}$, whereas time runs over $t = 1, \ldots, T-1$ in (12c) and $t = 2, \ldots, T-1$ in (12c)-(12d). The optimization variables are defined as

$$z_l(t) := [z_{l0}(t), z_{l1}(t), z_{l2}(t)]^T, \quad l \in \mathcal{G}, \, t \in \mathcal{T}, \text{ and}$$

$$x(t) := \big[\lambda^{min}(t)^T, \lambda^{max}(t)^T, \eta^{min}(t)^T, \eta^{max}(t)^T, \mu^{min}(t)^T, \mu^{max}(t)^T, \gamma^{min}(t)^T, \gamma^{max}(t)^T, \rho^{min}(t)^T, \rho^{max}(t)^T, \xi^{min}(t)^T, \xi^{max}(t)^T\big]^T.$$

The cost function is

$$\begin{aligned} h(x, z, \sigma, \beta) := & -\sum_{t \in \mathcal{T}} \sum_{l \in \mathcal{G}} z_{l2}(t) - \sum_{k \in \mathcal{N}} \beta_k \mathfrak{g}_k \\ & + \sum_{t \in \mathcal{T}} \sum_{k \in \mathcal{N}} \Big\{ \Lambda_k(t) P_k^d(t) + H_k(t) Q_k^d(t) + \lambda_k^{min}(t) P_k^{min} \\ & - \lambda_k^{max}(t) P_k^{max} + \eta_k^{min}(t) Q_k^{min} - \eta_k^{max}(t) Q_k^{max} \\ & + \mu_k^{min}(t) \left(V_k^{min}\right)^2 - \mu_k^{max}(t) \left(V_k^{max}\right)^2 + \rho_k^{min}(t) R_k^{min} \\ & - \rho_k^{max}(t) R_k^{max} + \xi_k^{min}(t) S_k^{min} - \xi_k^{max}(t) S_k^{max} - \gamma_k^{max}(t) B_k^{max} \Big\}, \end{aligned}$$

where, for $t \in \mathcal{T}$,

$$\Lambda_k(t) := \begin{cases} \lambda_k^{max}(t) - \lambda_k^{min}(t) \\ \qquad + c_{k1}(t) + 2\sqrt{c_{k2}(t)} z_{k1}(t), & k \in \mathcal{G}, \\ \lambda_k^{max}(t) - \lambda_k^{min}(t), & k \in \mathcal{N} \backslash \mathcal{G}, \end{cases}$$

$$H_k(t) := \eta_k^{max}(t) - \eta_k^{min}(t), \quad k \in \mathcal{N},$$

$$\Upsilon_k(t) := \mu_k^{max}(t) - \mu_k^{min}(t), \quad k \in \mathcal{N}.$$

Theorem 1: Optimization (11)-(12) is a Lagrangian dual of optimization (9)-(10) excluding the rank constraint (10k) and strong duality holds.

Proof: Introduce the following correspondence between the constraints in (10) (all constraints on reals written as $f(y) \leq 0$ with $f : \mathbb{R}^\nu \to \mathbb{R}$ and all constraints on symmetric matrices written as $f(y) \preceq 0$ with $f : \mathbb{R}^\nu \to \mathbb{R}^{\omega \times \omega}$) and the decision variables in (11)-(12).

$$\begin{array}{ll} \lambda_k^{max}(t), \lambda_k^{min}(t) \geq 0 & \text{for (10a)}, \\ \eta_k^{max}(t), \eta_k^{min}(t) \geq 0 & \text{for (10b)}, \\ \mu_k^{max}(t), \mu_k^{min}(t) \geq 0 & \text{for (10c)}, \\ \gamma_k^{max}(t), \gamma_k^{min}(t) \geq 0 & \text{for (10d)}, \\ \rho_k^{max}(t), \rho_k^{min}(t) \geq 0 & \text{for (10e)}, \\ \xi_k^{max}(t), \xi_k^{min}(t) \geq 0 & \text{for (10f)}, \end{array}$$

where, variables with the superscript "max" ("min") correspond to the upper (lower) bounds and the indices k and t run over the sets indicated in (10). For $k \in \mathcal{N}$ and $t = 1, \ldots, T-1$, $\sigma_k(t+1)$ corresponds to the equality constraint (10g), and β_k corresponds to that in (10h). Finally, let

$$\left[\begin{array}{cc} z_{l0}(t) & z_{l1}(t) \\ z_{l1}(t) & z_{l2}(t) \end{array} \right] \succeq 0$$

correspond to (10i) and $\Omega(t) \succeq 0$ correspond to (10j). Minimization of the Lagrangian with respect to $\alpha_l(t)$ leads to $z_{l0}(t) = 1$. Then, through elimination of $\Omega(t)$ and standard manipulations on the Lagrangian of optimization (9)-(10) (with the dual variables defined above), one can show that optimization (11)-(12) is a Lagrangian dual of optimization (9)-(10) excluding the rank constraint (10k). To show that strong duality holds, note that both optimization problems (11)-(12) and (9)-(10) excluding the rank constraint in (10k) are convex. A strictly feasible solution can be constructed as

$$\lambda_k^{min}(t) := \begin{cases} c_{k1}(t) + 1, & \text{for } k \in \mathcal{G} \\ 1, & \text{for } k \in \mathcal{N} \backslash \mathcal{G} \end{cases}$$

and $\lambda_k^{max}(t) = 1$, $\eta_k^{max}(t) = \eta_k^{min}(t) = 1$, $\mu_k^{max}(t) = 2$, $\mu_k^{min}(t) = 1$, $\rho_k^{max}(t) = \rho_k^{min}(t) = 1$, $\gamma_k^{max}(t) = \gamma_k^{min}(t) = 1$ $\xi_k^{max}(t) = \xi_k^{min}(t) = 1$, and $\beta_k = 0$, for $k \in \mathcal{N}$, $t \in \mathcal{T}$ along with $z_{l0}(t) = 0$, $z_{l1}(t) = 1$ for $l \in \mathcal{G}$ and $t \in \mathcal{T}$ and $\sigma_k(t+1) = 0$ for $k \in \mathcal{N}$ and $t \in \{0, \ldots, T-1\}$. Hence, strong duality holds by Slater's theorem [8].

Remark 2: Equation (12) shows that adding affine charge/discharge dynamics to the OPF problem does not change the structure of the dual variable that provides the basis for the main result in [23], [24]. This fact is the key to the constructing a solution to (8) from that of (11)-(12) using the procedure detailed in Section III-B. It should, however, be noted that the time dependence of each term in (12a) implies that the condition must hold at every $t \in \mathcal{T}$.

B. Constructing an optimal solution for OPF with storage

Theorem 1 shows that there is no duality gap between optimization (11)-(12) and a rank relaxation of the (equivalently) reformulated OPF problem with storage (9)-(10). Now, we show that under certain assumptions, there is no duality gap between the optimizations in (11)-(12) and (9)-(10).

Assumptions:

1) Optimization (9)-(10) is feasible and every feasible solution satisfies $W(t) \neq 0$ for all $t \in \mathcal{T}$.
2) There exists an optimal solution to (11)-(12) with optimal values $(x^{opt}(t), z^{opt}(t))$ for $(x(t), z(t))$ such that

$$A^{opt}(t) := \sum_{k \in \mathcal{N}} \left[\Lambda_k^{opt}(t) \mathbf{Y}_k + H_k^{opt}(t) \overline{\mathbf{Y}}_k + \Upsilon_k^{opt}(t) M_k \right]$$

has a zero eigenvalue of multiplicity two for $t \in \mathcal{T}$.

Remark 3: Assumption 1 is to avoid trivial solutions and implies that $V(t) = 0$ is not feasible for (9)-(10), or for the equivalent optimization (8), for any $t \in \mathcal{T}$.

Remark 4: Assumption 2 is critical for constructing a solution to (9)-(10) from the solution of (11)-(12) (using the KKT condition $\text{tr}(W^{opt}(t) A^{opt}(t)) = 0$ at each $t \in \mathcal{T}$). Note that Assumption 2 can only be verified once the problem in (11)-(12) has been solved. Moreover, it limits the instances of the problem in (9)-(10) for which a solution can be constructed. References [23], [24] discuss algebraic and geometric interpretations of Assumption 2 under the extra condition that Y is symmetric with nonnegative off-diagonal entries in $\text{Re}(Y)$ and nonpositive off-diagonal entries in $\text{Im}(Y)$.

Theorem 2: Under Assumptions 1 and 2, $\varphi^* = \psi^*$ and an optimal solution to (9)-(10) (and equivalently for (8)) can be constructed from the solution of (11)-(12).

The proof of Theorem 2 is a straightforward extension of Theorem 1 in [23], which is a similar result for the OPF problem without storage dynamics.

C. Summary of the computational procedure

We now summarize how the results described above can be used to compute a solution to (8) by solving the problem in (11)-(12). Given a feasible solution to (11)-(12) that satisfies Assumption 2 and some $[\nu_1(t)^T \ \nu_2(t)^T]^T$, with $\nu_1(t), \ \nu_2(t) \in \mathbb{R}^n$, in the null space of $A^{opt}(t)$. An optimal value $V^{opt}(t)$ for $V(t)$ can be computed as

$$V^{opt}(t) = (\zeta_1(t) + \zeta_2(t)\mathbf{i})(\nu_1(t) + \nu_2(t)\mathbf{i}),$$

where the constants $\zeta_1(t)$ and $\zeta_2(t)$ can be determined from the KKT conditions $\mu_k^{min}(t)((V_k^{min})^2 - |V_k(t)|^2) = 0$ and $\mu_k^{max}(t)(|V_k(t)|^2 - (V_k^{max})^2) = 0$ along with the fact that the phase angle at the swing (reference) bus is known (e.g., zero). This optimal $V^{opt}(t)$ can then be used to compute $W(t)$. Finally, optimal values for P^g, Q^g, b, r, and s are computed through the KKT conditions at each $k \in \mathcal{N}$,

$$\begin{array}{c} \lambda_k^{min}(t) \left[\text{tr}\{\mathbf{Y}_k W(t)\} + r_k(t) - P_k^{min} + P_k^d(t) \right] = 0, \\ \lambda_k^{max}(t) \left[P_k^{max} - P_k^d(t) - \text{tr}\{\mathbf{Y}_k W(t)\} - r_k(t) \right] = 0, \\ \eta_k^{min}(t) \left[\text{tr}\{\overline{\mathbf{Y}}_k W(t)\} + s_k(t) - Q_k^{min} + Q_k^d(t) \right] = 0, \\ \eta_k^{max}(t) \left[Q_k^{max} - Q_k^d(t) - \text{tr}\{\overline{\mathbf{Y}}_k W(t)\} - s_k(t) \right] = 0, \\ \gamma_k^{min}(t) b_k(t) = 0, \qquad \gamma_k^{max}(t) \left[B_k^{max} - b_k(t) \right] = 0, \end{array}$$

for $t \in \mathcal{T}$ and

$$\begin{array}{c} \rho_k^{min}(t) \left[r_k(t) - R_k^{min} \right] = 0, \quad \rho_k^{max}(t) \left[R_k^{max} - r_k(t) \right] = 0, \\ \xi_k^{min}(t) \left[s_k(t) - S_k^{min} \right] = 0, \quad \xi_k^{max}(t) \left[S_k^{max} - s_k(t) \right] = 0, \\ \sigma_k(t+1) \left[r_k(t) - b_k(t+1) + b_k(t) \right] = 0, \end{array}$$

for $t = 1, \ldots, T-1$, and $\beta_k \left[b_k(1) - \mathfrak{g}_k \right] = 0$ along with the reformulations of (6). Note that the KKT conditions constitute

a set of affine equality constraints on the decision variables P^g, Q^g, b, r, and s.

If the optimal value of the optimization in (11)-(12) is unbounded, the problem in (8) is infeasible (because the rank relaxation of the equivalent reformulation in (9)-(10) is infeasible). However, if the problem in (11)-(12) is feasible but its solution violates Assumption 2, then the procedure is inconclusive (i.e., an optimal solution for the optimization in (8) cannot be guaranteed).

Remark 5: The optimization problems in this paper (e.g., that in (11)-(12)) are solved using the parser YALMIP [25] and the solver SeDuMi [33] in the Matlab environment. Efficient computations for optimization in (11)-(12) that may exploit the structure of the constraints (e.g., recursion over time) are subjects of ongoing research.

IV. Case studies

In this section, we illustrate the effects of energy storage using IEEE benchmark systems [34] with different cost functions of the form (8) using the solution procedure discussed in Section III-B and III-C. The simulations discussed herein were performed on both the IEEE 14 and 30 bus benchmark systems. However, since there was no qualitative difference in the trends observed, only the results from the 14 bus test system, which represents a portion of the Midwestern US Electric Power System as of February, 1962 [34], are reported here. Neither of the benchmark systems include storage. Therefore, while we use their network topology as well as their voltage and generation bounds, (i.e., V^{max}, V^{min}, P^{max}, P^{min}, Q^{max} and Q^{min} in (1) and (2)), appropriate values for the storage parameters along with time-varying demand profiles need to be estimated. Demand profiles for each bus are created using typical hourly demands for 14 (or 30) different 2009 December days in Long Beach, CA, USA [1]. The curves are scaled so that their peak corresponds to the static demand values in the IEEE 14 (or 30) bus test case. Figure 2(a) shows the demand curves for each bus for the 14 bus case. For all of the results presented here the rate limits in (5) are set to be between $25-33\%$ of the maximum capacity of the storage, e.g. $0.25B_{max}\Delta t$ with $\Delta t = 1$ with units of Mega Watts (MW). The limits S_k^{max} and S_k^{min} in (7) on the reactive power are set to keep the rate angle between $-18\deg$ and $48\deg$. This range was selected based on the real and reactive generation limits in the IEEE 14 bus test case which give rise to generator angles approximately between $-17\deg$ and $90\deg$. Unless otherwise indicated all power values reported in the following sections are normalized to per unit values (p.u.) as described in [26].

A. Example I: Linear cost

We first use a cost function that is the sum of the total generation (i.e., $\|P^g\|_1 = \sum_{t=1}^{T}\sum_{l\in\mathcal{G}} P_l^g(t)$) and refer to this as a time-invariant linear cost function since the coefficients $c_{l1}(t) = 1$ and $c_{l2}(t) = 0$ from (8) are constant in time for each $l \in \mathcal{G}$. Figure 2(b) shows that the addition of storage (32 MWh per bus) as well as the finite-horizon optimization produces a flatter generation curve over the time period. This change is most evident for generators 4 and 5 (respectively P_4^g and P_5^g). For this cost function, the optimal solution did not make use of generator 1. A constant generation profile is desirable from an operator perspective as the efficiency of most conventional generators are optimized for full capacity. As a result, many operators maintain generation levels that will accommodate the peak demand which can lead to excess power being curtailed.

There has been a great deal of research aimed at demand-based pricing strategies, (i.e., higher prices at peak demand times). In order to simulate this effect we use a weighted ℓ_1 norm (i.e., $\sum_{t=1}^{T}\sum_{l\in\mathcal{G}} c_{l1}(t)P_l^g(t)$) for the cost function in (8). The peak normalized demand profiles provided in the top panel of Figure 5(b) show that $t = 15$ is roughly the time step where the average demand starts to increase toward peak levels. Accordingly, we set $c_{l1}(t) = 1$ for $t \in \{1,\dots 15\}$ and $c_{l1}(t) = 1.5$ for $t \in \{16,\dots 24\}$ for each $l \in \mathcal{G}$ and refer to the weighted ℓ_1 norm with these coefficients as the time-varying (or demand-based) linear cost function.

Figure 2(b) shows that the time-varying linear cost function further regulates the demand profile to an essentially constant level for generators 4 and 5 and reduces the peak-to-trough spread on generator 2. Generator 1 also provides a small amount of generation during the peak period. It should be noted that generators 2 and 3 produce power primarily to track their own load, for both the time-invariant and time-varying linear cost functions. One reason that the optimal solution to this OPF with storage does flatten all of the generation profiles is that the linear cost function (i.e., ℓ_1 norm based) attempts to minimize overall generation rather than the total energy of the power signal.

Figure 3(a) shows results obtained using the time-varying linear cost function at two additional storage levels. The reduction in the generation peak begins with storage levels as low as 6 MWh per bus, which corresponds to a storage capacity that can handle 2% of the full daily demand or 33% of the peak load. It should be noted that the optimal solutions computed for all of the results based on linear cost functions favor storage at only the non-generating nodes. Therefore, the actual storage use represents 1.4% of the system capacity or 21% of the peak load. The reason that the storage use is distributed in this manner and the general problem of optimal storage placement is a topic of ongoing study [7], [31]. As expected, the benefit of the storage increases with storage capacity. The relationship between added storage capacity and reductions in the overall system load is illustrated in Figure 3(b), which shows the aggregated system demand and generation with 6, 12 and 32 MWh of per-bus storage using the time-varying linear cost function, that is also used in Figure 3(a). These curves correspond to 5.4%, 9.2% and 20.3% peak reductions for respective additions of 6, 12 and 32 MWh of per-bus storage capacity or 54, 108 and 288 MWh of respective storage use. (As previously noted, only the capacity at the load buses is used.) These trends provide insight into the peak-shaving potential that can be realized through investing in various amounts of storage capacity.

Figure 4(a) shows how the optimal cost function value changes with per-bus storage capacity B_k^{max} in MWh for the linear cost function with both time-invariant and time-varying

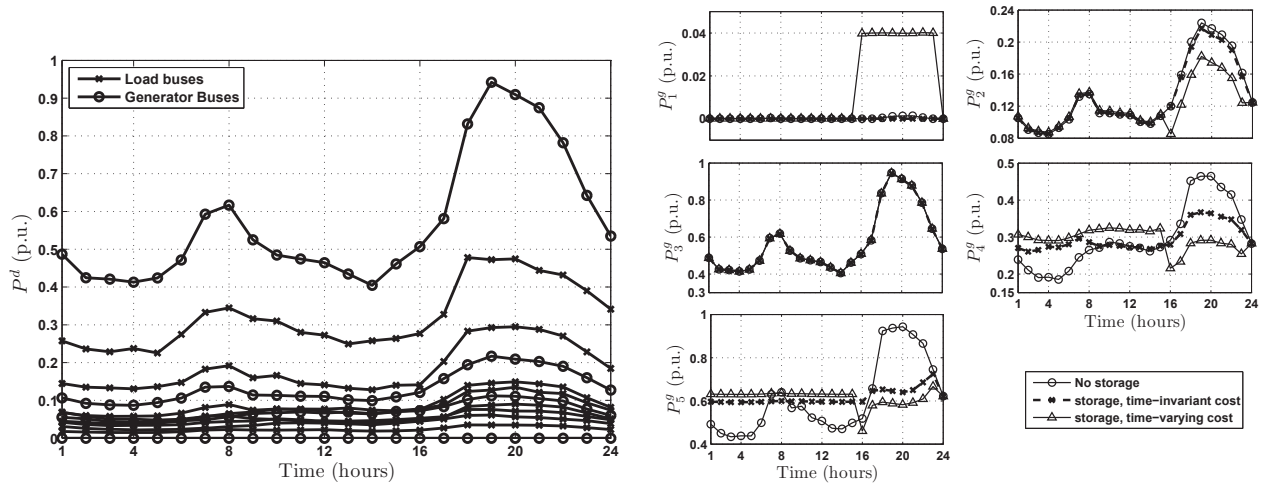

(a) (b)

Fig. 2. (a) Hourly demand curves for the 14 bus case that are peak scaled to match the static demands from the IEEE 14 bus benchmark system. The load profiles represent demands for 14 different typical 2009 December days in Long Beach, CA, USA. (b) Hourly generation for each $l \in \mathcal{G}$. The addition of 32 MWh storage at each bus as well as optimization over time results in flatter generation profiles, especially when a demand-based time-varying cost function is used. This smoothing of the generation curve is most evident for generators 4 and 5. Generators 2 and 3 produce power primarily to track their own load when the cost function is linear.

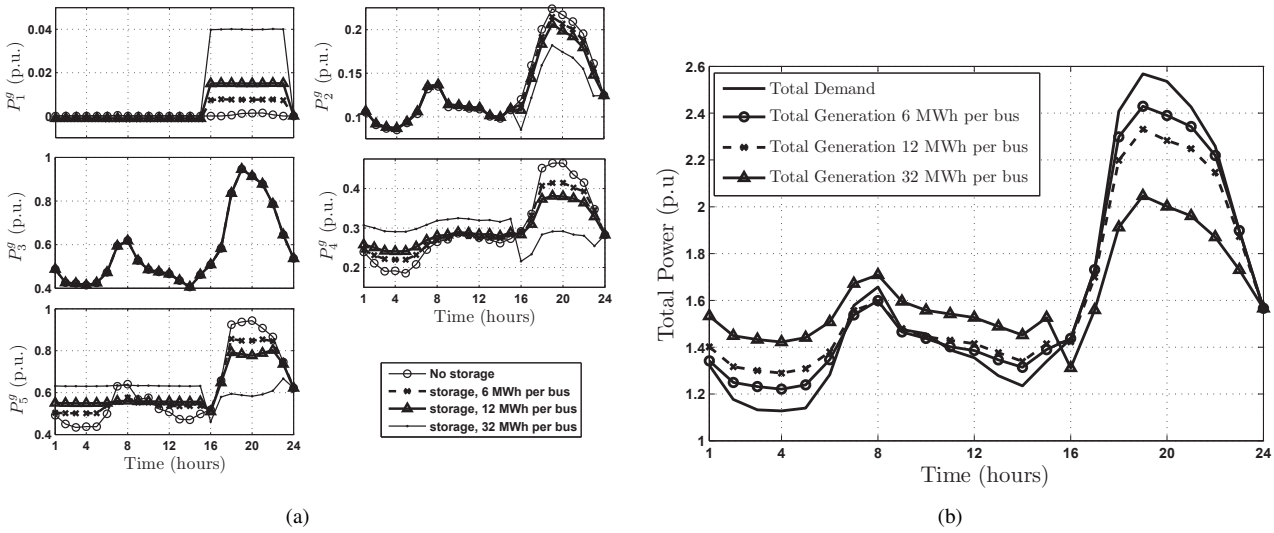

(a) (b)

Fig. 3. (a) Hourly generation for each $l \in \mathcal{G}$ given a time-varying (demand-based) linear cost function over a range of per-bus storage levels. (b) Aggregated hourly generation as a function of per-bus storage compared with the total demand. There is a clear trade-off between the amount of peak load the generators need to supply and the required per-bus storage capacity. As expected, increasing the level of per-bus storage decreases the generation peaks but even low levels of storage effectively lower the peak. Note that the benefits gained by increasing per-bus storage capacity does not continue indefinitely as is shown through the saturation in Figure 4(a). For all storage levels this smoothing of the generation curve is most evident for generators 4 and 5, whereas generators 2 and 3 produce power primarily to track their own load.

coefficients with the values normalized so that each $P_l^g(t)$ for $l \in \mathcal{G}$ and $t \in \mathcal{T}$ is a p.u. value. For the time-independent cost function the storage reduces the cost (in this case, total generation) by only a small amount. While, the addition of a simple demand-based cost structure increases the storage's cost benefit by about 0.8% for every additional 8 MWh of per-bus storage capacity.

B. Example II: Quadratic cost

In this subsection, we repeat the computations described in Section IV-A for both time-invariant and time-varying quadratic cost functions. Again, we use higher cost function coefficients for $t \geq 15$ to reflect a demand-based pricing scheme. For all cases the second-order coefficients are those of the IEEE 14 bus test case [34], which are $c_{l2}(t) = 0.043$, $c_{22}(t) = 0.250$, $c_{l2} = 0.01$ for $l = 3, 4, 5$ all over time steps $t = 1, \ldots, 24$. The linear coefficients were selected to maintain the ratio of costs between the generators in the test case. This led to time-invariant linear coefficients of $c_{l1}(t) = 2$ for $l = 1, 2$, and $c_{l1}(t) = 4$ for $l = 3, 4, 5$ over time steps $t = 1, \ldots, 24$ and time-varying first-order coefficients of $c_{l1}(t) = 2$ for $l = 1, 2$ and $c_{l1}(t) = 4$ for $l = 3, 4, 5$ over times $t = 1, \ldots, 15$, and $c_{l1}(t) = 4$ for $l = 1, 2$ and $c_{l1}(t) = 8$

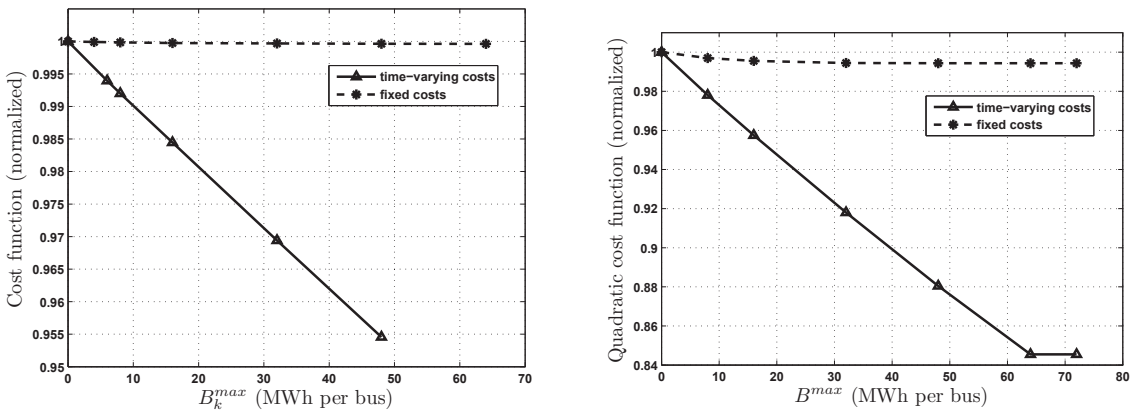

(a) (b)

Fig. 4. Cost versus per-bus storage capacity (B_k^{max} in MWh). (a) Linear cost function. (b) Quadratic cost function. In all cases, the cost decreases with increased storage capacity and this decrease is roughly linear (as a function of per-bus storage capacity) for the cost functions with time-varying coefficients.

for $l = 3, 4, 5$ when $t = 16, \ldots, 24$.

Figure 4(b) indicates that the addition of storage visibly reduces the quadratic cost function value even when the coefficients are tim independent. The reduction is roughly 0.3% for the first 8 MWh of per-bus storage capacity and then the added savings with increasing amounts of storage drops off rapidly especially at per-bus storage capacities greater than 32 MWh. As with the linear cost function, the value for the time-varying case decreases approximately linearly with increasing storage. However, the slope is significantly steeper with each additional 8 MWh of per-bus storage capacity reducing the cost function value by roughly 2% until we reach a limit beyond which additional storage no longer affects the cost function value (at approximately 64 MWh of per-bus capacity).

Figure 5(a) shows that a quadratic time-varying cost function further flattens the generation profiles and this effect increases as the per-bus storage capacity is increased. For the quadratic time-varying costs, generators 1 and 2 provide all of the required power. In the following, we refer to the remaining 12 nodes (i.e., including those with generators that are not used) as non-generating nodes. Clearly, the form of the cost function favors the use of the first two generators. The addition of storage and an optimization over time produce almost constant levels of generation for generator 1 over the 24 hour period when compared to the no-storage case. At the highest storage capacity (32 MWh per bus) the power range for generator 2 is reduced from $[0.24, 0.71]$ to $[0.30, 0.54]$.

Figure 5(b) shows the relationship between storage use and demand for the demand-based quadratic cost function. The top panel reflects peak normalized demand at each bus with the average per-bus demand (excluding buses with no demand) superimposed with a thick dashed-line. The center and lower panels reflect the storage use with two different per-bus capacity constraints (respectively, $B_k^{max} = 32$ MWh and $B_k^{max} = 72$ MWh). As the demand increases, the storage is charged until the time increment before the first local peak (at $t = 8$), then the storage is used to reduce the generation load until the demand stabilizes. Finally, the storage is recharged until the peak load (at $t = 18$), and then discharged until the end of the day. For the higher storage capacity constraint ($B_k^{max} = 72$ MWh) the storage is never fully charged. The maximum per-bus usage is approximately 64 MWh, which explains why the cost function value does not change for the last two points (per-bus B^{max} levels) on Figure 4(b).

As discussed in Section IV-A the optimal solution corresponds to storage use only at the non-generating nodes, i.e., some of the capacity is not being used. This fact is illustrated using Figure 6, which shows the aggregate system storage for both the linear and quadratic cost function when $B_k^{max} = 12$ MWh for $k \in \mathcal{N}$ with the full system, non-generating and load-only node aggregate capacities indicated. Similar results hold for all of the storage capacities that were studied and this phenomena is being investigated as part of a larger ongoing study related to optimal storage placement, see e.g. [7], [31].

Remark 6: It was observed in [23] that Assumption 2 in Section III-B is satisfied in many of the IEEE benchmark systems when a small amount of resistance (e.g., of the order of 10^{-5} per unit) was added to each transformer. In the numerical examples in this paper, we implement this modification. This modification essentially renders the graph induced by $\mathrm{Re}(Y)$ strongly connected.

V. Summary and potential extensions

We investigated the effects of storage capacity and power rating on generation costs and peak reductions using a modified version of the IEEE 14 and 30 bus benchmark systems. In order to carry out these investigations we formulated an OPF problem with simple charge/discharge dynamics for energy storage as a finite-time optimal control problem. The resulting optimization problem, under certain conditions (discussed in the previous sections), was solved using a procedure based on a convex SDP obtained as a Lagrangian dual to the rank relaxation of an equivalent formulation for the OPF problem with storage dynamics.

As discussed in the earlier sections, the motivation of the current work is to assess the utility of grid-integrated storage in mitigating issues associated with integrating intermittent renewable energy resources into the electric power grid. As

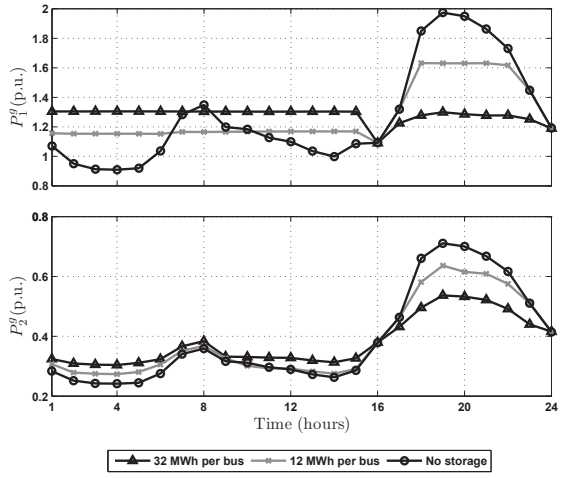

(a)

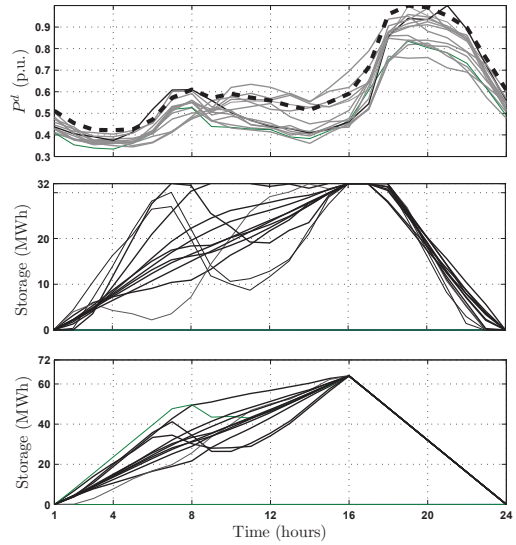

(b)

Fig. 5. (a) Generation comparison for $B^{max} = 12$ and $B^{max} = 32$ MWh of per-bus storage versus no storage with a quadratic time-varying cost function. Generators 3–5 do not generate power in any scenario. (b) The top panel shows the peak normalized demand. At $t = 15$, the average demand excluding buses with no demand (shown as the thick dashed-line) starts to increase toward peak levels, this defines the point where the cost function coefficients are increased to reflect a demand-based pricing scheme. The center and lower panels respectively show the storage use for the same cost function as in (a) based on per-bus capacity constraints of 32 and 72 MWh respectively. For the higher storage capacity, the full capacity is not used at any of the nodes.

a step toward this goal, the current paper investigated only the impact of large scale integration of energy storage. Adding uncertainties due to either intermittency in generation or fluctuations in demand is a subject of ongoing study (with preliminary work reported in [31]). Another natural extension is assessing the use of energy storage systems to minimize grid level losses and reduce the need for transmission capacity expansion.

Energy storage can provide the power system with flexibility for dealing with a number of concerns including power quality,

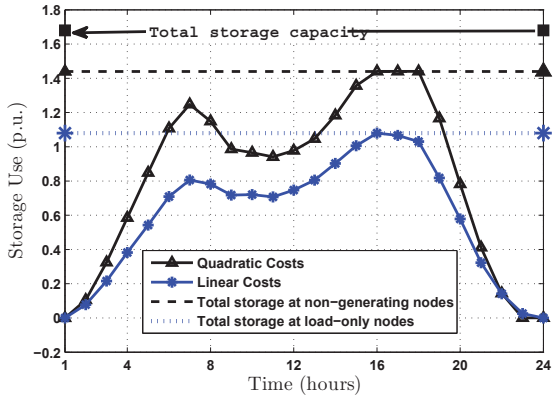

Fig. 6. An illustration of total system storage use for simulations with both linear and quadratic cost functions versus storage capacity for the full system with $B^{max} = 12$ MWh at each bus. The dashed line at 1.44 p.u. represents the total storage capacity over the 12 nodes where there is no generation and the dotted line at 1.08 p.u. represents the total generation at all load only buses. As illustrated in Figure 5(a) only 2 of the 5 generators actually provide power when a quadratic cost function is used therefore we denote the remaining 12 nodes as non-generating nodes.

stability, load following, peak reduction, and reliability. A promising direction for future work is assessing the suitability of hybrid storage technologies (e.g., a combination of pumped-hydro, thermal, and batteries) in addressing these issues. Spinning reserves and/or conventional generators with high ramp rates can provide similar services, thus an interesting design issue is determining the appropriate balance between storage and ancillary generation capacities.

ACKNOWLEDGEMENTS

The authors gratefully acknowledge George Rodriguez and Christopher Clarke of Southern California Edison as well as K. Mani Chandy of the California Institute of Technology for fruitful discussions and helpful suggestions.

REFERENCES

[1] Personal communication with Southern California Edison researchers.
[2] T. Ackerman, Ed., *Wind Power in Power Systems*. Wiley, 2005.
[3] N. Alguacil and A. J. Conejo, "Multiperiod optimal power flow using Benders' decomposition," *IEEE Trans. on Power Systems*, vol. 15, no. 1, pp. 196 –201, 2000.
[4] Y. M. Atwa and E. F. El-Saadany, "Optimal allocation of ESS in distribution systems with a high penetration of wind energy," *IEEE Trans. on Power Systems*, vol. 25, no. 4, pp. 1815–1822, Nov. 2010.
[5] X. Bai, H. Wei, K. Fujisawa, and Y. Wang, "Semidefinite programming for optimal power flow problems," *Int'l J. of Electrical Power & Energy Systems*, vol. 30, no. 6-7, pp. 383–392, 2008.
[6] J. P. Barton and D. G. Infield, "Energy storage and its use with intermittent renewable energy," *IEEE Trans. on Energy Conversion*, vol. 19, no. 2, pp. 441–448, 2004.
[7] S. Bose, D. F. Gayme, U. Topcu, and K. M. Chandy, "Optimal placement of energy storage in the grid," *to appear in Proc. of Conf. on Decision and Control*, 2012.
[8] S. Boyd and L. Vandenberghe, *Convex Optimization*. Cambridge Univ. Press, 2004.
[9] V. Budhraja, F. Mobasheri, M. Cheng, J. Dyer, E. Castano, S. Hess, and J. Eto, "California's electricity generation and transmission interconnection needs under alternative scenarios," California Energy Commission, Tech. Rep., 2004.
[10] J. Carpentier, "Contribution to the economic dispatch problem," *Bulletin de la Societe Francoise des Electriciens*, vol. 3, no. 8, pp. 431–447, 1962, in French.

[11] J. M. Carrasco, L. G. Franquelo, J. T. Bialasiewicz, E. Galván, R. C. Portillo Guisado, M. A. Martí Prats, J. León, and N. Moreno-Alfonso, "Power-electronic systems for the grid integration of renewable energy sources: A survey," *IEEE Trans. on Industrial Electronics*, vol. 53, no. 4, pp. 1002–1016, 2006.

[12] K. M. Chandy, S. Low, U. Topcu, and H. Xu, "A simple optimal power flow model with energy storage," in *Proc. of Conf. on Decision and Control*, 2010.

[13] H. P. Chao and S. Peck, "A market mechanism for electric power transmission," *J. of Regulatory Economics*, vol. 10, pp. 25–59, 1996.

[14] H. P. Chao, S. Peck, S. Oren, and R. Wilson, "Flow-based transmission rights and congestion management," *The Electricity J.*, vol. 13, no. 8, pp. 38–58, 2000.

[15] M. Geidl and G. Andersson, "A modeling and optimization approach for multiple energy carrier power flow," in *Proc. of IEEE PES PowerTech*, 2005.

[16] I. P. Gyuk, "EPRI-DOE handbook of energy storage for transmission and distribution applications," EPRI-DOE, Washington, DC, Tech. Rep., December 2003.

[17] K. Heussen, S. Koch, A. Ulbig, and G. Andersson, "Energy storage in power system operation : The power nodes modeling framework," in *IEEE PES Conference on Innovative Smart Grid Technologies Europe*. IEEE, 2010, pp. 1–8.

[18] W. W. Hogan, "Contract networks for electric power transmission," *J. of Regulatory Economics*, vol. 4, no. 3, pp. 211–42, 1992.

[19] M. Huneault and F. D. Galiana, "A survey of the optimal power flow literature," *IEEE Trans. on Power Systems*, vol. 6, no. 2, pp. 762–770, 1991.

[20] R. Jabr, "Radial distribution load flow using conic programming," *IEEE Trans. on Power Systems*, vol. 21, no. 3, pp. 1458–1459, Aug. 2006.

[21] ——, "Optimal power flow using an extended conic quadratic formulation," *IEEE Trans. on Power Systems*, vol. 23, no. 3, pp. 1000–1008, Aug. 2008.

[22] J. Lavaei, "Zero duality gap for classical OPF problem convexifies fundamental nonlinear power problems," in *Proc. of the American Control Conf.*, 2011.

[23] J. Lavaei and S. Low, "Convexification of optimal power flow problem," in *Proc. of Allerton Conf. on Communication, Control and Computing*, 2010.

[24] ——, "Zero duality gap in optimal power flow problem," *IEEE Trans. on Power Systems*, vol. 27, Feb. 2012.

[25] J. Löfberg, "YALMIP : A toolbox for modeling and optimization in MATLAB," in *Proc. of the CACSD Conf.*, Taipei, Taiwan, 2004. [Online]. Available: http://control.ee.ethz.ch/~joloef/yalmip.php

[26] J. A. Momoh, *Electric Power System Applications of Optimization*, ser. Power Engineering, H. L. Willis, Ed. Markel Dekker Inc.: New York, USA, 2001.

[27] J. A. Momoh, M. E. El-Hawary, and R. Adapa, "A review of selected optimal power flow literature to 1993. Part I: Nonlinear and quadratic programming approaches," *IEEE Trans. on Power Systems*, vol. 14, no. 1, pp. 96–104, 1999.

[28] K. S. Pandya and S. K. Joshi, "A survey of optimal power flow methods," *J. of Theoretical and Applied Information Technology*, vol. 4, no. 5, pp. 450–458, 2008.

[29] R. Schainker, "Executive overview: Energy storage options for a sustainable energy future," in *Proc. of IEEE PES General Meeting*, 2004, pp. 2309–2314.

[30] S. M. Schoenung, J. M. Eyer, J. J. Iannucci, and S. A. Horgan, "Energy storage for a competitive power market," *Ann. Rev. of Energy and the Environment*, vol. 21, no. 1, pp. 347–370, 1996.

[31] A. E. Sjödin, D. F. Gayme, and U. Topcu, "Risk-mitigated optimal power flow for wind powered grids," in *Proc.of the American Control Conf.*, 2012.

[32] E. Sortomme and M. A. El-Sharkawi, "Optimal power flow for a system of microgrids with controllable loads and battery storage," in *Power Systems Conf. and Exposition*, 2009.

[33] J. Sturm, "Using SeDuMi 1.02, a MATLAB toolbox for optimization over symmetric cones," *Optimization Methods and Software*, vol. 11, no. 1-4, pp. 625–653, 1999.

[34] University of Washington, "Power systems test case archive." [Online]. Available: http://www.ee.washington.edu/research/pstca/

[35] U.S. Energy Information Administration, "Annual energy outlooks 2010 with projections to 2035," U.S. Department of Energy, Tech. Rep. DOE/EIA-0383, 2010. [Online]. Available: http://www.eia.doe.gov/oiaf/aeo

[36] P. Vytelingum, T. D. Voice, S. D. Ramchurn, A. Rogers, and N. R. Jennings, "Agent-based micro-storage management for the smart grid," in *The Ninth Int'l Conf. on Autonomous Agents and Multiagent System*, Toronto, May 2010, pp. 39–46.

[37] H. Xu, U. Topcu, S. Low, and K. M. Chandy, "On load-shedding probabilities of power systems with renewable power generation and energy storage," in *Proc. Allerton Conf. on Communication, Control and Computing*, 2010.

[38] T. Yau, L. Walker, H. Graham, and A. Gupta, "Effects of battery storage devices on power system dispatch," *IEEE Trans. on Power Apparatus and Systems*, vol. PAS-100, no. 1, pp. 375–383, 1981.

[39] R. D. Zimmerman, C. E. Murillo-Sánchez, and R. J. Thomas, "MATPOWER's extensible optimal power flow architecture," in *Proc. IEEE PES General Meeting*, 2009, pp. 1–7.

Dennice Gayme is an Assistant Professor in the Department of Mechanical Engineering at Johns Hopkins University. She was previously a postdoctoral scholar in the Computing & Mathematical Sciences Department at the California Institute of Technology (Caltech). She received her doctorate in Control and Dynamical Systems in 2010 from CalTech where she was a recipient of the P.E.O. scholar award in 2007 and the James Irvine Foundation Graduate Fellowship in 2003. She received a Master of Science from the University of California at Berkeley in 1998 and a Bachelor of Engineering & Society from McMaster University in 1997 both in Mechanical Engineering. Prior to her doctoral work she was a Senior Research Scientist in the Systems and Control Technology and Vehicle Health Monitoring Groups at Honeywell Laboratories from 1999-2003. Dennice's research interests are in the study of large-scale interconnected systems with an emphasis on renewable and efficient energy systems and wall turbulence.

Ufuk Topcu is a postdoctoral scholar of Control and Dynamical Systems at the California Institute of Technology. He received his Ph.D. in 2008 from the University of California, Berkeley. His research is on the analysis, design, and verification of networked, information-based systems. Current projects are in energy networks, advanced air vehicle architectures, and autonomy.